Geophysical Research Letters

RESEARCH LETTER
10.1029/2024GL108462

Atmospheric pCO_2 Response to Stimulated Organic Carbon Export: Sensitivity Patterns and Timescales

Mark Holzer[1], **Tim DeVries**[2,3], **and Benoît Pasquier**[1]

[1]Department of Applied Mathematics, School of Mathematics and Statistics, University of New South Wales, Sydney, NSW, Australia, [2]Department of Geography, University of California, Santa Barbara, CA, USA, [3]Earth Research Institute, University of California, Santa Barbara, CA, USA

Key Points:

- pCO_2 sensitivity to carbon export perturbations is governed by sequestration time, preformed response time, and atmospheric turnover time
- High sensitivity occurs in the tropics and Southern Ocean where sequestration time is long and preformed response time is short
- The preformed response time is modulated by air-sea CO_2 disequilibrium and shortest in the Atlantic and Southern Ocean

Supporting Information:

Supporting Information may be found in the online version of this article.

Correspondence to:

M. Holzer,
mholzer@unsw.edu.au

Citation:

Holzer, M., DeVries, T., & Pasquier, B. (2024). Atmospheric pCO_2 response to stimulated organic carbon export: Sensitivity patterns and timescales. *Geophysical Research Letters*, *51*, e2024GL108462. https://doi.org/10.1029/2024GL108462

Received 23 JAN 2024
Accepted 23 MAY 2024

Author Contributions:

Conceptualization: Mark Holzer, Tim DeVries, Benoît Pasquier
Formal analysis: Mark Holzer, Tim DeVries, Benoît Pasquier
Funding acquisition: Mark Holzer
Investigation: Mark Holzer, Tim DeVries, Benoît Pasquier
Methodology: Mark Holzer, Tim DeVries, Benoît Pasquier
Resources: Mark Holzer
Software: Mark Holzer, Benoît Pasquier
Validation: Mark Holzer, Tim DeVries, Benoît Pasquier
Writing – original draft: Mark Holzer

Abstract The ocean's organic carbon export is a key control on atmospheric pCO_2 and stimulating this export could potentially mitigate climate change. We use a data-constrained model to calculate the sensitivity of atmospheric pCO_2 to local changes in export using an adjoint approach. A perpetual enhancement of the biological pump's export by 0.1 PgC/yr could achieve a roughly 1% reduction in pCO_2 at average sensitivity. The sensitivity varies roughly 5-fold across different ocean regions and is proportional to the difference between the mean sequestration time τ_{seq} of regenerated carbon and the response time τ_{pre} of performed carbon, which is the reduction in the preformed carbon inventory per unit increase in local export production. Air-sea CO_2 disequilibrium modulates the geographic pattern of τ_{pre}, causing particularly high sensitivities (2–3 times the global mean) in the Antarctic Divergence region of the Southern Ocean.

Plain Language Summary Atmospheric CO_2 levels could be reduced by stimulating plankton in the ocean to produce more organic carbon that then sinks to depth (is exported) at a higher rate. The resulting carbon deficit in surface waters drives atmospheric carbon into the ocean. The efficacy of this process depends on how long the exported carbon stays isolated from the surface and how quickly the surface deficit can be filled. Here we investigate how sensitive atmospheric CO_2 levels are to a given enhancement in carbon export and where such enhancements would be most effective. We show that the sensitivity is determined by the difference between the time for which exported carbon stays sequestered at depth and the time with which the rest of the carbon in the ocean responds to the additional export rate. High sequestration times are found where the organic carbon is exported into old deep waters, while fast response times are found where it is easy for gas exchange to inject carbon into the ocean and where the additionally exported carbon is less likely to resurface and escape into the atmosphere. These factors result in the Southern Ocean and the tropics having greatest sensitivity.

1. Introduction

Carbon sequestration in the ocean is a major control on atmospheric CO_2 (e.g., Ducklow et al., 2001) and hence on the radiative forcing of the climate system. A key mechanism for ocean carbon sequestration is the biological pump, which removes dissolved inorganic carbon (DIC) from the surface ocean through photosynthesis and exports organic carbon to depth where it is respired to DIC that remains sequestered for decades to centuries (e.g., DeVries et al., 2012; Holzer et al., 2021; Nowicki et al., 2022). Without the biological pump, atmospheric CO_2 concentrations would have been about 200 ppm higher even in preindustrial times (e.g., Volk & Hoffert, 1985). The importance of the biological pump for atmospheric CO_2 has focused intense interest on the inner workings of the biological pump (e.g., Siegel et al., 2016) and how it might respond to changes in the marine environment (e.g., Boyd, 2015; Henson et al., 2022; J. K. Moore et al., 2018; Pasquier, Holzer, & Chamberlain, 2023). To combat accelerating climate change, deliberate manipulation of the biological pump is now being considered as a strategy for carbon dioxide removal (CDR) from the atmosphere (e.g., Gattuso et al., 2021; NASEM, 2019). Enhancing organic carbon export to depth will lower atmospheric CO_2 concentrations, raising the question as to where such enhancement is most effective and how much CO_2 reduction is possible for a given export enhancement.

Here we ask how the atmospheric CO_2 concentration responds in steady state to permanent local perturbations in the biological pump. Perturbations in export could occur naturally as the system adjusts to changes in the macronutrient supply (e.g., Liu et al., 2023) or to changing micronutrients such as iron (e.g., Ito et al., 2016), or they could be deliberate through direct sustained fertilization (e.g., Buesseler et al., 2004; Hauck et al., 2016),

Writing – review & editing: Mark Holzer, Tim DeVries, Benoît Pasquier

manipulation of the light supply (Irvine et al., 2016), or other geo-engineering approaches aimed at enhancing the biological pump for CDR. We quantify the response of atmospheric CO_2 to permanent steady-state export perturbations in terms of a linear sensitivity in the spirit of what has been done for the sensitivity to dissolved iron perturbations (Dutkiewicz et al., 2006) and recently for the sensitivity of the ocean's oxygen content to biological production changes (Holzer, 2022). We generally expect higher sensitivity for regions where exported carbon stays sequestered at depth longer, as this means that the surface DIC deficit maintained by enhanced export is larger, leading to a greater drawdown of atmospheric CO_2 (e.g., Kwon et al., 2009). However, the sequestration time alone is unlikely to completely determine the sensitivity pattern because surface disequilibrium modifies both the rate at which atmospheric CO_2 replaces the DIC deficit and the rate at which resurfacing regenerated DIC can escape back into the atmosphere (Eggleston & Galbraith, 2018; Ito & Follows, 2013). Importantly, sequestration time alone cannot determine the magnitude of the sensitivity, which depends not only on carbon export but also on air-sea CO_2 exchange.

2. Methods

We use an optimized steady-state model of the ocean's carbon, phosphorus, and oxygen cycles (PCO2, Pasquier, Holzer, Chamberlain, Matear, et al., 2023) embedded in a steady data-assimilated ocean circulation model (OCIM2, DeVries, 2014; DeVries & Holzer, 2019), which has a resolution of $2° \times 2°$ with 24 vertical levels. In the version of PCO2 employed here, the ocean exchanges CO_2 with the atmosphere, modeled as a single well-mixed reservoir. The atmospheric CO_2 mixing ratio is determined from conservation of carbon by the atmosphere-ocean system; changes in the terrestrial carbon pool are neglected for simplicity. The model does not include the nitrogen cycle, but a nitrate contribution to total alkalinity (TA) is parameterized using a fixed nitrate-to-phosphate stoichiometry (Wolf-Gladrow et al., 2007). Photosynthetic organic-carbon production at rate U is modeled as proportional to phosphate (PO_4) uptake with variable C:P stoichiometry (Galbraith & Martiny, 2015) and parameterized in terms of PO_4 and light colimitation and temperature though a simple logistic model of phytoplankton mortality (Pasquier & Holzer, 2017). Photosynthesis takes place only in the model euphotic zone defined by a 1% threshold of photosynthetically active radiation as used in the ACCESS-1.3 climate model (Bi et al., 2013). Organic-carbon production is routed, in fixed globally uniform proportions, to rapidly ("fast") and slowly sinking particulate organic carbon (POCf and POCs), and to semi-labile dissolved organic carbon (DOC).

The model state is determined by the concentrations of DIC, POCf, POCs, particulate inorganic carbon, DOC, PO_4, oxygen, and TA, whose grid values are organized into vectors. If χ denotes the concatenated tracer concentration vectors, the biogeochemical steady state is the solution to

$$F(\chi, U) = 0, \tag{1}$$

where the organic-carbon production rate per unit volume U is a function of χ, and F is the vector of tracer tendencies set to zero for steady state. The nonlinear Equation 1 is solved using a Newton method (e.g., Kelley, 2003; also Pasquier, Holzer, Chamberlain, Matear, et al., 2023).

We stimulate the biological soft-tissue pump by considering, separately for each euphotic grid box, enhancements in the POC production U_{POC} per unit volume. (DOC production and export are not perturbed.) After perturbing U_{POC} in a given euphotic grid cell by δU, we calculate a new steady state of the system, that is, we determine the steady-state response to permanent changes δU. In the limit of small-amplitude perturbations δU, the tracer response $\delta\chi$ can be computed from the linearization

$$\frac{\partial F}{\partial \chi}\delta\chi + \frac{\partial F}{\partial U}\delta U = 0, \tag{2}$$

where the partial derivatives and U are evaluated at the model's base state (U is held fixed at its unperturbed values everywhere except in the grid box where U is enhanced by adding POC-production perturbation δU). Organizing the partial derivatives of Equation 2 into matrices $\mathbf{J} = \partial F/\partial\chi$ and $\mathbf{M} = \partial F/\partial U$, and collecting the production perturbations for every euphotic grid cell into the columns of diagonal matrix $\delta\mathbf{U}$ (every column containing the perturbed production of the corresponding single euphotic grid box), we have

$$\delta\chi = -\mathbf{J}^{-1}\,\mathbf{M}\,\delta\mathbf{U}. \tag{3}$$

Each column of $\delta\chi$ represents a tracer solution for every column of $\delta\mathbf{U}$, with as many columns as there are euphotic grid points. Because we are only interested in the response of the atmospheric carbon inventory, or equivalently of the total ocean carbon content, we use the adjoint of Equation 3 and solve a single linear system for the volume integral of $\delta\chi$ (Text S1 in Supporting Information S1).

In the linear limit of small-amplitude δU, the response in carbon inventories is proportional to δU. U itself is poorly constrained by the observations because rapid recycling in the euphotic zone does not impact the DIC concentrations against which the model is optimized. For this reason, we quantify the magnitude of the perturbations in terms of the export production per unit volume ϕ_{ex}, which strongly influences tracer concentrations and is therefore directly constrained by the optimization. Moreover, POC export rates are in principle available through direct measurement and changes in these rates are a robust metric of biological pump changes. We therefore normalize the response of the system to a perturbation in a given grid box, identified by its position $\mathbf{r}$, by the change in export production $\delta\phi_{ex}(\mathbf{r})$, where the export production $\phi_{ex}(\mathbf{r})$ is defined as the globally integrated aphotic respiration rate of organic carbon that was produced at $\mathbf{r}$ per unit volume (Primeau et al., 2013). (In practice ϕ_{ex} and $\delta\phi_{ex}$ are calculated using an adjoint approach; Text S1 in Supporting Information S1.) The perturbation $\delta\phi_{ex}(\mathbf{r})$ has a dominant component directly proportional to $\delta U(\mathbf{r})$ and in principle also contributions from the perturbed oxygen field, but the oxygen component is negligible (Text S1 in Supporting Information S1).

To eliminate dependence on grid size, we calculate all perturbations and responses per unit perturbation volume, that is, per unit volume of the grid box where production and export are perturbed. Specifically, if C_{atm} and C_{ocn} are the atmospheric and oceanic carbon inventories, with responses $\delta C_{atm}(\mathbf{r})$ and $\delta C_{ocn}(\mathbf{r})$ to perturbations in volume element $dV(\mathbf{r})$, we calculate the per-unit-perturbation-volume responses $\delta\mu_{atm}(\mathbf{r}) = \delta C_{atm}(\mathbf{r})/dV(\mathbf{r})$ and $\delta\mu_{ocn}(\mathbf{r}) = \delta C_{ocn}(\mathbf{r})/dV(\mathbf{r})$. Similarly, for the gross CO_2 flux across the sea surface Φ_{as}, we use the per-unit-perturbation-volume response $\delta\phi_{as}(\mathbf{r}) = \delta\Phi_{as}/dV(\mathbf{r})$ so that $\delta\phi_{as}$ and $\delta\phi_{ex}$ have the same dimensions. [Φ_{as} is the globally integrated gross air-sea flux $k\ pCO_2$ (e.g., Friedlingstein et al., 2023), while the net air-sea flux is $k\left(pCO_2 - pCO_2^{ocn}\right)$, where pCO_2^{ocn} is the effective partial pressure of dissolved CO_2 and k is the local gas-exchange coefficient.] Note that for all these quantities the $\mathbf{r}$ dependence signifies the dependence on where the perturbation is applied. The quantities $\delta\mu_{ocn}$, $\delta\mu_{atm}$, $\delta\phi_{ex}$, and $\delta\phi_{as}$ are all per-unit-volume intensive quantities; if export is perturbed over a larger region, the total changes are obtained by volume integrating with respect to $\mathbf{r}$.

3. Sensitivity Metric and Relation to Key Timescales

The central quantity of interest is the change in atmospheric carbon inventory per unit export perturbation, that is, $\delta\mu_{atm}(\mathbf{r})/\delta\phi_{ex}(\mathbf{r})$, at every point $\mathbf{r}$ in the euphotic zone. $\delta\mu_{atm}(\mathbf{r})/\delta\phi_{ex}(\mathbf{r})$ has dimensions of time and is proportional to the atmospheric turnover time $\tau_{atm} = C_{atm}/\Phi_{as} = \delta\mu_{atm}/\delta\phi_{as}$, where the last equality follows because both C_{atm} and Φ_{as} are proportional to atmospheric pCO_2. We thus have

$$\frac{\delta\mu_{atm}}{\delta\phi_{ex}} = -\tau_{atm}\,S \qquad \text{with} \qquad S \equiv -\frac{\delta\phi_{as}}{\delta\phi_{ex}}, \tag{4}$$

where we have defined the *flux-sensitivity ratio* S, and the atmospheric turnover time is $\tau_{atm} = 9.6$ years for our model with an atmospheric carbon inventory of 593 PgC (CO_2 at 278 ppm) and a gross air-sea flux of 62 PgC/yr. The negative sign is introduced so that $S > 0$, as for positive $\delta\phi_{ex}$ both $\delta\phi_{as}$ and $\delta\mu_{atm}$ are negative (reduction in atmospheric CO_2). S can be considered the fundamental dimensionless metric of the sensitivity.

Given $S(\mathbf{r})$ and the export perturbation field $\delta\phi(\mathbf{r})$, the response of atmospheric pCO_2 is readily available. Because the gas-exchange coefficients (pressure-weighted global integral K) do not change in response to biological perturbations, and with $\Phi_{as} = K\ pCO_2$, it follows that $\delta pCO_2/pCO_2 = \delta\Phi_{as}/\Phi_{as}$. With $\delta\Phi_{as} = \int\delta\phi_{as}\,dV$ and $\delta\phi_{as} = -S\,\delta\phi_{ex}$ by definition (Equation 4), we have

$$\frac{\delta pCO_2}{pCO_2} = -\frac{\int S(\mathbf{r})\delta\phi_{ex}(\mathbf{r})\,dV}{\Phi_{as}} = -\bar{S}\,\frac{\delta\Phi_{ex}}{\Phi_{as}}, \tag{5}$$

where $\delta\Phi_{ex} = \int \delta\phi_{ex}\, dV$ and $\bar{S}$ is the $\delta\phi_{ex}$-weighted volume average of S. In terms of typical numbers, if a hypothetical volume-integrated export enhancement were to be $\delta\Phi_{ex} \sim 0.1$ PgC/yr with $\bar{S} \sim 6$, then the fractional change $\delta pCO_2/pCO_2 \sim -6\,(0.1/62) \sim -1\%$. For steady states with higher atmospheric CO_2 concentrations, Φ_{as} and to a good approximation the global-mean S scale linearly with atmospheric pCO_2 implying a similar fractional change in pCO_2 for a given export perturbation.

Enhanced export production increases the ocean's regenerated DIC inventory and at the same time reduces its preformed DIC inventory. If there were no atmosphere, the regenerated increase and preformed reduction would match exactly. With the atmosphere present, reduced surface DIC drives an influx of atmospheric CO_2 that lessens the reduction of the preformed DIC inventory. To analyze this quantitatively, we decompose the response of the ocean's carbon inventory $\delta\mu_{ocn}$ into the changes of the preformed and regenerated DIC inventories, that is, $\delta\mu_{ocn} = \delta\mu_{pre} + \delta\mu_{reg}$, where we omitted the negligible response of carbon tied up in POC and DOC. (For perturbations of both POC and DOC export, the DOC term is important as discussed in Text S1 of Supporting Information S1.) Conservation of carbon by the atmosphere-ocean system, $-\delta\mu_{atm} = \delta\mu_{ocn}$, then means that

$$-\frac{\delta\mu_{atm}}{\delta\phi_{ex}} = \frac{\delta\mu_{reg}}{\delta\phi_{ex}} + \frac{\delta\mu_{pre}}{\delta\phi_{ex}}, \tag{6}$$

where every term has the dimensions of time. The left-hand side becomes $S\,\tau_{atm}$ from Equation 4. $\delta\mu_{reg}/\delta\phi_{ex} = \tau_{seq}$ is the sequestration time, which is the mean time that exported carbon stays sequestered below the euphotic zone as regenerated DIC (Boyd et al., 2019; DeVries et al., 2012; Holzer et al., 2021; Siegel et al., 2021). An alternative definition of τ_{seq} in terms of the time taken for biogenic DIC to equilibrate with the atmosphere was recently proposed by Nowicki et al. (2024), which accounts for the effects of slow air-sea CO_2 equilibration on biogenic carbon sequestration. Here, we maintain the original definition of τ_{seq} and account for the influence of air-sea disequilibrium by its effect on the preformed carbon inventory as discussed below.

We define the preformed response time $\tau_{pre} \equiv -\delta\mu_{pre}/\delta\phi_{ex}$, which is the reduction in the preformed DIC inventory per unit increase in export flux, and hence simply the bulk timescale with which the export perturbation would flush out the response of the preformed DIC inventory. An interpretation of τ_{pre} in terms of a mean residence time of labeled carbon (as is the case for τ_{seq} and τ_{atm}) is not available to the best of our knowledge. However, τ_{pre} as defined here is a convenient timescale for characterizing the preformed DIC response, while τ_{seq} is the natural timescale for characterizing the export perturbation. Conservation of carbon as expressed by Equation 6 relates the flux-sensitivity ratio S to these timescales through

$$S = \frac{\tau_{seq} - \tau_{pre}}{\tau_{atm}}. \tag{7}$$

High sensitivity thus corresponds to long τ_{seq} and/or short τ_{pre}. Note that $\delta\mu_{pre}$ can at most be as large in magnitude as $\delta\mu_{reg}$, which would occur in the limit of no gas exchange when the preformed DIC deficit is entirely "filled" by resurfacing regenerated DIC. This guarantees that $\tau_{seq} \geq \tau_{pre}$, thus ensuring $S \geq 0$.

4. Magnitude and Patterns of the Sensitivity

Figure 1a shows a map of the euphotic-mean flux-sensitivity ratio S. The largest sensitivities occur in the polar Southern Ocean, tropical oceans, subpolar Pacific and North Atlantic. The global mean of S is 5, with the peak sensitivities occurring in the Southern Ocean where S exceeds 14. Figures 1b and 1c show euphotic-mean maps of τ_{seq} and τ_{pre}. Comparison with Figure 1a shows that to a first approximation the geographic pattern of S is set by τ_{seq}. High τ_{seq} occurs where exported organic carbon is injected into slowly ventilated or old waters such as the tropical eastern Pacific, and where deep-water formation in the North Atlantic and Southern Ocean transports exported carbon into the deep ocean (DeVries et al., 2012; Holzer et al., 2021; Nowicki et al., 2022). The response time τ_{pre} has a similar pattern as τ_{seq} but is generally shorter (by 47 years in the global mean) due to the invasion of atmospheric carbon, which fills some of the preformed DIC deficit created by the export anomaly. If the sea surface were impermeable (no gas exchange) τ_{pre} and τ_{seq} would be identical in both pattern and magnitude. If air-sea exchange were instantaneous allowing surface waters everywhere to equilibrate with the atmosphere, air-sea exchange would have almost no influence on the pattern of τ_{pre} which would thus be expected to be nearly identical to that of τ_{seq} except for modest modulations due to variations in the Revelle buffer factor (Revelle &

10.1029/2024GL108462

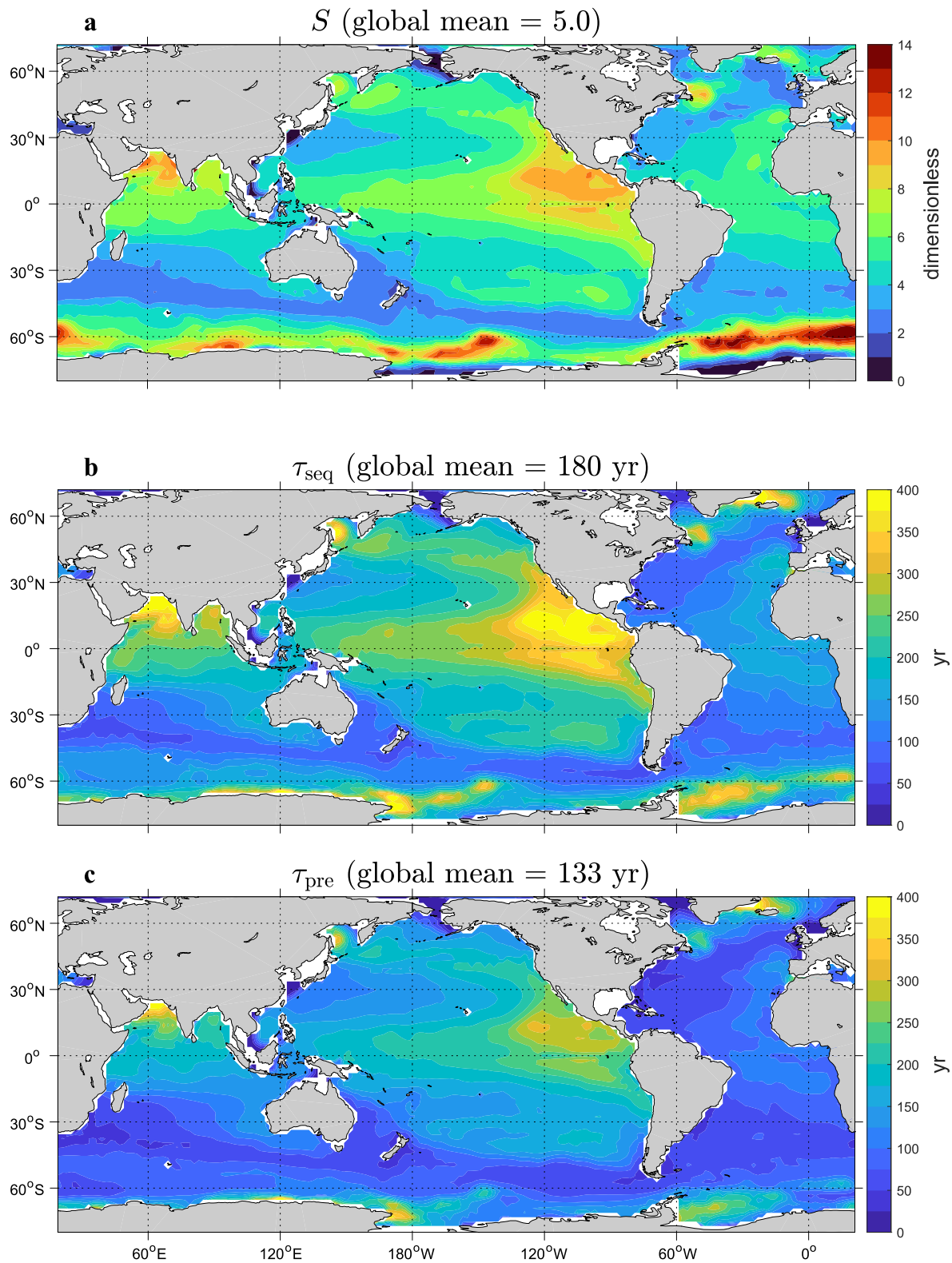

Figure 1. (a) Euphotic vertical means of the dimensionless flux-sensitivity ratio $S = -\delta\phi_{as}/\delta\phi_{ex}$, (b) the mean sequestration time τ_{seq}, and (c) the preformed response time τ_{pre}. (Latitudes north of 72°N are not shown due to the model's coarse resolution there producing potential numerical artifacts.)

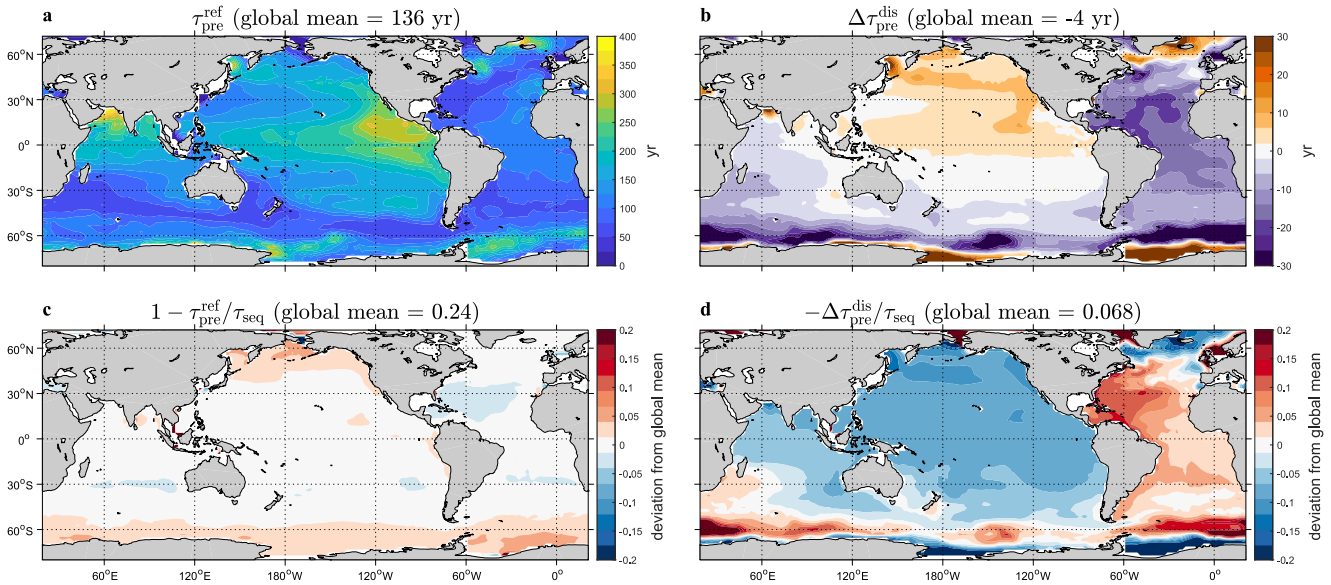

Figure 2. (a) The euphotic vertical mean of the reference and (b) disequilibrium components of the preformed response time τ_{pre}. To quantify how these contribute to the pattern of the flux-sensitivity ratio S relative to that of the sequestration time τ_{seq}, panel (c) shows $1-\tau^{ref}_{pre}/\tau_{seq}$ and panel (d) shows $-\Delta\tau^{dis}_{pre}/\tau_{seq}$, which can be added to give the ratio $\tau_{atm}\,S/\tau_{seq}$.

Suess, 1957). For the real ocean, the circulation and mixing often do not allow waters to linger in contact with the atmosphere long enough for DIC to equilibrate.

How do the broadly similar patterns of S, τ_{seq}, and τ_{pre} differ in detail and what is the role of air-sea disequilibrium? To investigate this, we partition τ_{pre} into a rapid-gas-exchange reference value τ^{ref}_{pre} and a disequilibrium contribution $\Delta\tau^{dis}_{pre}=\tau_{pre}-\tau^{ref}_{pre}$, which can have either sign (e.g., Marinov et al., 2008; Toggweiler et al., 2003). We compute τ^{ref}_{pre} by performing the sensitivity calculation with the gas-exchange coefficients set so large that air-sea exchange is near-instantaneous (we use uniform coefficients set to 10^4 times the maximum realistic value).

To quantify how the pattern of S differs from that of τ_{seq} and how disequilibrium contributes to the differences, we consider ratios with τ_{seq} and rewrite Equation 7 as $\tau_{atm}\,S/\tau_{seq}=\left(1-\tau^{ref}_{pre}/\tau_{seq}\right)-\Delta\tau^{dis}_{pre}/\tau_{seq}$. The euphotic-mean terms of this equation are plotted in Figure 2 together with maps of τ^{ref}_{pre} and $\Delta\tau^{dis}_{pre}$. Figures 2a and 2c show that τ^{ref}_{pre} is the dominant contributor to the amplitude of S, but the pattern of τ^{ref}_{pre} barely differs from that of τ_{seq}. Weak variations in $\tau^{ref}_{pre}/\tau_{seq}$ are consistent with those of the Revelle buffer factor (e.g., Holzer & DeVries, 2022; Sabine et al., 2004). A smaller than average buffer factor at low latitudes means that a given reduction in atmospheric pCO_2 equilibrates with a higher DIC response, and hence a higher τ^{ref}_{pre} and a lower value of $\left(1-\tau^{ref}_{pre}/\tau_{reg}\right)$. The converse is true at high latitudes where the buffer factor is larger than average.

The disequilibrium term shown in Figure 2d contributes only about 10% to the global mean sensitivity (-4 years out of $\tau_{atm}\,\bar{S}\sim 48$ yr) but is important locally in modulating the pattern of S relative to that of τ_{seq}. Negative $\Delta\tau^{dis}_{pre}$ is most pronounced in the Atlantic and Southern Ocean (Figures 2b and 2d), indicating that there τ_{pre} is shorter, giving a larger sensitivity S. Short τ_{pre}, that is, a small response in the preformed DIC inventory, occurs when the negative preformed DIC anomaly continually created by stimulated export is effectively erased (Figure 3): Effective erasure through the invasion of atmospheric CO_2 is achieved when the negative surface preformed DIC anomalies in the vicinity of the perturbation equilibrate quickly with the atmosphere (low disequilibrium), and when the positive preformed DIC anomalies due to resurfacing regenerated DIC are prevented from equilibrating (high disequilibrium) and escaping back into the atmosphere. Because organic carbon is generally respired with a surface-intensified profile (approximately a power law, Martin et al., 1987), most of the regenerated DIC resurfaces near the export perturbation, mitigating the effect of disequilibrium which has opposing effects on invasion and escape. Deep regenerated DIC that resurfaces far from the point of export tends to do so preferentially

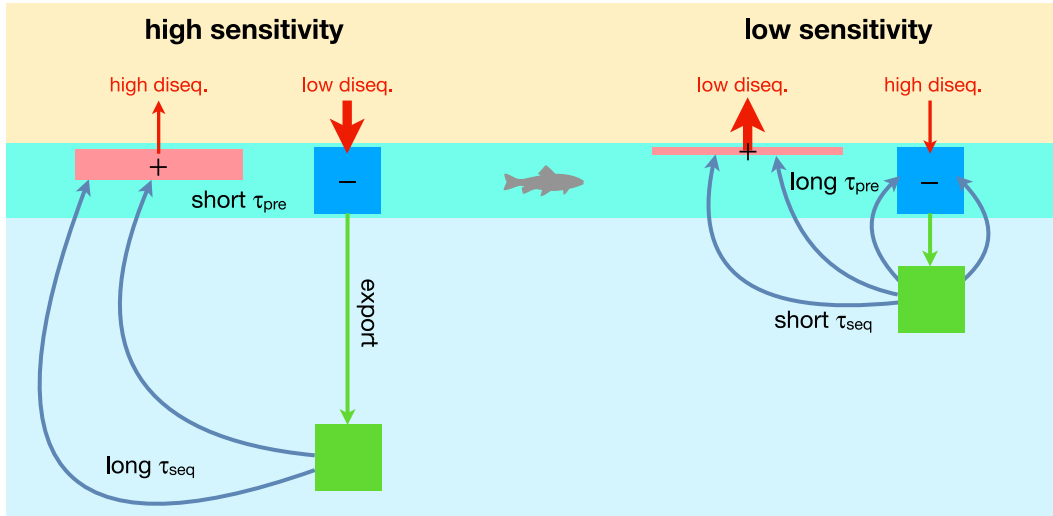

Figure 3. Schematic to contrast conditions leading to high or low sensitivity of atmospheric CO_2 to local steady-state export enhancement. Permanently enhanced export continually creates a negative anomaly in surface dissolved inorganic carbon (DIC) (blue box) in the vicinity of the perturbation, and a positive surface DIC anomaly where regenerated DIC upwells to the surface (reddish box). High sensitivity of atmospheric CO_2 to the export perturbation occurs where the sequestration time of exported carbon is long, which gives atmospheric carbon time to invade before regenerated DIC resurfaces and erases the negative preformed DIC anomaly. Air-sea disequilibrium enhances this sensitivity if it occurs where regenerated DIC resurfaces, but reduces the sensitivity if it occurs in the region where the export perturbation is applied.

in the Southern Ocean (Nowicki et al., 2024), especially for DIC regenerated in the Atlantic and in the Southern Ocean itself. The Southern Ocean is a region of rapid overturning and mixing and hence characterized by high disequilibrium, which is consistent with smaller values of τ_{pre} for Atlantic and Southern Ocean perturbations.

Figure 2b shows that $\Delta\tau_{pre}^{dis}$ is strongly positive (~30 years or more) in deep-water formation regions (Ross, Weddell, Labrador, Greenland seas) and slightly positive in the North Pacific (less than ~10 years). In these regions τ_{pre} is thus longer than the equilibrated reference value, meaning reduced effectiveness of the atmosphere at erasing the negative preformed DIC anomaly, which indicates disequilibrium for invasion. (Because the rapid-gas-exchange reference state has virtually zero disequilibrium, $\Delta\tau_{pre}^{dis} > 0$ cannot mean yet lower disequilibrium for escape.) The pattern of positive $\Delta\tau_{pre}^{dis}$ is consistent with the expectation of high disequilibrium for the deep-water formation regions and for ice-covered seas, where the negative preformed DIC anomaly from stimulated export is either rapidly subducted and mixed away from the surface or physically shielded from the atmosphere. In agreement with these findings, Nowicki et al. (2024) also found that air-sea disequilibrium reduces the amount of DIC sequestered by organic carbon export in deep-water formation regions. The slightly positive $\Delta\tau_{pre}^{dis}$ in the North Pacific indicates less sensitivity than in the reference case and must therefore be associated with modest disequilibrium proximal to the North Pacific perturbations.

To support these interpretations of $\Delta\tau_{pre}^{dis}$, we examined the response in net air-sea carbon flux for Atlantic and Pacific export perturbations, and Atlantic perturbations indeed tend to outgas more in the Southern Ocean (Figure S1 in Supporting Information S1). To confirm the key role of Southern Ocean disequilibrium in controlling τ_{pre}, we recomputed $\Delta\tau_{pre}^{dis}$ for the hypothetical case with near-instantaneous air-sea exchange south of 40°S. Relieving surface disequilibrium in the Southern Ocean reduces the negative values of $\Delta\tau_{pre}^{dis}$ in the North Atlantic by a factor of roughly 2, while leaving the positive values of $\Delta\tau_{pre}^{dis}$ in the North Atlantic largely unchanged (Figure S2 in Supporting Information S1).

The ratio between S and τ_{seq} (the sum of the terms plotted in Figures 2c and 2d) quantifies the effect of the preformed response time in modifying the pattern of S from that of τ_{seq}; a uniform ratio would indicate identical patterns. The ratio shows that S is enhanced relative to τ_{seq} by up to about 40% in the Atlantic and even more in the Southern Ocean, with corresponding reductions elsewhere. Thus, the effect of the preformed response time, dominantly through its disequilibrium contribution, is to enhance the sensitivity in the Atlantic and Southern

Oceans outside the deep-water formation regions of the polar/sub-polar North Atlantic and Antarctic margin. This enhancement, as quantified by $-\Delta\tau^{dis}_{pre}/\tau_{seq}$, is particularly pronounced in the Antarctic Divergence region (Figure 2d). Here, a large fraction of the positive subsurface DIC anomalies created by enhanced export upwell into a region of intense air-sea disequilibrium, preventing their equilibration with the atmosphere and thus enhancing the sensitivity S (Figure 3). Elsewhere in the tropical and subtropical Atlantic, sensitivity is also enhanced but to a lesser degree because a smaller fraction of the regenerated DIC anomaly from these regions upwells into the Antarctic Divergence.

5. Discussion

The sensitivity patterns calculated here are relevant for marine CDR strategies, such as iron fertilization (e.g., Buesseler et al., 2004; Hauck et al., 2016), that seek to draw down atmospheric CO_2 by stimulating the biological pump. Our results show that the average flux-sensitivity ratio S is about 5, which translates to roughly a 1% drawdown in atmospheric CO_2 for a 0.1 PgC/yr permanent export enhancement. However, S varies widely across the ocean, ranging from 2 to 4 in the sub-Antarctic and the western North Atlantic and North Pacific, to 8–10 in the equatorial Pacific and Indian Ocean, and >12 in the Antarctic Divergence region of the Southern Ocean. The equatorial Pacific and Southern Ocean are both iron-limited regions (C. M. Moore et al., 2013) that would be conducive to iron fertilization (e.g., Aumont & Bopp, 2006). If carbon export were enhanced in these regions where $S \sim 10$, then atmospheric CO_2 would decrease by 2% for a 0.1 PgC/yr export increase. The main reason for enhanced sensitivity in the tropical Pacific and Indian Ocean is their long sequestration time, while air-sea disequilibrium significantly enhances the sensitivity in the Antarctic Divergence region. Sensitivity declines sharply to the north and south of the Antarctic Divergence, indicating that fertilization north of the polar front or along the Antarctic margin would not be effective. The sharp divide to the north of the polar front has previously been termed the Southern Ocean "biogeochemical divide" (Marinov et al., 2006). The divide toward the Antarctic margin is from air-sea disequilibrium preventing the ingassing of atmospheric CO_2 in response to enhanced export along the Antarctic margin, due to rapid deep convection and sea ice in this region.

The steady-state sensitivities and timescales calculated here can be regarded as fundamental metrics of the carbon cycle obtained from a linearization about the current ocean state. While sensitivities were calculated for preindustrial CO_2 concentrations as these were approximately steady, the response $\delta pCO_2/pCO_2$ (see Equation 5) is insensitive to the equilibrium atmospheric CO_2 concentration (and hence to the Revelle buffer factor), and the OCIM2 circulation and biogeochemical parameters have been optimized against late-twentieth-century climatology. Thus, the sensitivities computed here are applicable to the climatological mean state of the modern ocean. However, the effects of seasonal to interannual variability on the preformed and regenerated DIC inventories are not captured by our steady-state model.

In terms of applicability to marine CDR, there are several caveats. First, we considered only the steady-state response to permanent perturbations in organic-carbon export. Because realistic export enhancements are unlikely to be sustained in perpetuity, the transient response to pulsed enhancements is more relevant to CDR. However, the same mechanisms and large-scale patterns identified here likely also shape the transient response. Realistic iron fertilization strategies would also have to consider changes in ocean state on the timescale of τ_{seq} as the ocean circulation and thermodynamic state are predicted to vary considerably over the next century (e.g., Weijer et al., 2020). For the time-dependent case one can still define a flux-sensitivity ratio as in Equation 4, and because it simply re-expresses carbon conservation by the atmosphere-ocean system Equation 7 still holds if there are no changes in terrestrial carbon storage. However, all timescales would become time dependent, requiring explicit time stepping of a different tracer for each euphotic grid box in a dynamic ocean model, which is beyond the scope of our study. Second, realistic export enhancements will stimulate both POC and DOC export. While our model represents only a single semi-labile DOC pool with a fixed 2-year lifetime, we find that when we perturb both POC and DOC export, the sensitivity is reduced (global mean $S = 3.6$) with both shorter values of τ_{seq} and τ_{pre}. Inclusion of perturbed DOC export further amplifies the differences between the patterns of S and τ_{seq} (Figures S3 and S4 in Supporting Information S1). Third, our study only applies to CDR approaches for which organic particles are exported naturally through gravitational settling. Export enhancements that involve artificial transport to the ocean bottom or that remove carbon from the atmosphere-ocean system are no longer solely governed by the biological pump and hence expected to have different sensitivities.

6. Conclusions

The sensitivity to export perturbations at any given point in the euphotic zone is naturally quantified by the dimensionless flux-sensitivity ratio S, which is the ratio of the response in the gross air-sea CO_2 flux to the perturbation in the organic-carbon export rate. For a given field of perturbed export $\delta\phi_{ex}$ the volume integral $\int S\ \delta\phi_{ex}\ dV$ provides the response of atmospheric pCO_2 through Equation 5. The global average of S is about 5 and at this value of sensitivity a 0.1 PgC/yr export enhancement would draw down atmospheric CO_2 by roughly 1%.

The geographic sensitivity pattern is dominantly determined by the sequestration time τ_{seq}, which is longest where export accesses slowly ventilated deep-water masses in the tropical eastern Pacific, and in the deep-water formation regions of the North Atlantic and Southern Ocean. The amplitude of the sensitivity is set by the difference between τ_{seq} and the preformed response time τ_{pre}. The preformed response time modulates the geographic sensitivity pattern primarily through the effects of air-sea CO_2 disequilibrium. This results in a sensitivity pattern with higher Southern Ocean sensitivity than what would be expected from the pattern of τ_{seq} alone, especially in a narrow band along the Antarctic Divergence.

Our analysis has highlighted the subtle interplay between carbon sequestration and air-sea exchange that determines the steady-state response of atmospheric carbon to perturbations in organic-carbon export. The timescales and patterns of the response are fundamental metrics of the global marine carbon cycle and should be useful for assessing carbon models as well as for potentially guiding future geo-engineering efforts for CDR to mitigate climate change.

Data Availability Statement

This research used the PCO_2 biogeochemistry model whose code is publicly available (Pasquier, 2023). The photosynthetically available radiation fields used by PCO_2 are from the "historical" ACCESS1.3 model runs publicly available as part of the Australian CMIP5 archive (NCI-ESGF, 2013). The OCIM2 transport matrix and corresponding salinity and temperature fields are publicly available at UCSB (DeVries, 2019). Sea-ice and surface-wind data are from the NCAR-NCEP Reanalysis 1 (Kalnay et al., 1996). Gridded observed silicic-acid concentrations used with the carbonate chemistry are from the World Ocean Atlas 2018 (Garcia et al., 2018).

Acknowledgments
We acknowledge funding from ARC Grant DP210101650 (MH) and NSF Grant OCE-1948955 (TD). Open access publishing facilitated by University of New South Wales, as part of the Wiley - University of New South Wales agreement via the Council of Australian University Librarians.

References

Aumont, O., & Bopp, L. (2006). Globalizing results from ocean in situ iron fertilization studies. *Global Biogeochemical Cycles*, *20*(2), GB2017. https://doi.org/10.1029/2005GB002591

Bi, D., Dix, M., Marsland, S., O'Farrell, S., Rashid, H., Uotila, P., et al. (2013). The ACCESS coupled model: Description, control climate and evaluation. *Australian Meteorological and Oceanographic Journal*, *63*(1), 41–64. https://doi.org/10.22499/2.6301.004

Boyd, P. W. (2015). Toward quantifying the response of the oceans' biological pump to climate change. *Frontiers in Marine Science*, *2*, 77. https://doi.org/10.3389/fmars.2015.00077

Boyd, P. W., Claustre, H., Levy, M., Siegel, D. A., & Weber, T. (2019). Multi-faceted particle pumps drive carbon sequestration in the ocean. *Nature*, *568*(7752), 327–335. https://doi.org/10.1038/s41586-019-1098-2

Buesseler, K. O., Andrews, J. E., Pike, S. M., & Charette, M. A. (2004). The effects of iron fertilization on carbon sequestration in the Southern Ocean. *Science*, *304*(5669), 414–417. https://doi.org/10.1126/science.1086895

DeVries, T. (2014). The oceanic anthropogenic CO_2 sink: Storage, air-sea fluxes, and transports over the industrial era. *Global Biogeochemical Cycles*, *28*(7), 631–647. https://doi.org/10.1002/2013GB004739

DeVries, T. (2019). OCIM2 transport matrix and ocean state [Dataset]. *UCSB Ocean Circulation and Biogeochemistry Lab*. https://tdevries.eri.ucsb.edu/models-and-data-products/

DeVries, T., & Holzer, M. (2019). Radiocarbon and helium isotope constraints on deep-ocean ventilation and mantle-^{3}He sources. *Journal of Geophysical Research: Oceans*, *124*(5), 3036–3057. https://doi.org/10.1002/2018JC014716

DeVries, T., Primeau, F., & Deutsch, C. (2012). The sequestration efficiency of the biological pump. *Geophysical Research Letters*, *39*(13), L13601. https://doi.org/10.1029/2012GL051963

Ducklow, H. W., Steinberg, D. K., & Buesseler, K. O. (2001). Upper ocean carbon export and the biological pump. *Oceanography*, *14*(4), 50–58. https://doi.org/10.5670/oceanog.2001.06

Dutkiewicz, S., Follows, M. J., Heimbach, P., & Marshall, J. (2006). Controls on ocean productivity and air-sea carbon flux: An adjoint model sensitivity study. *Geophysical Research Letters*, *33*(2), L02603. https://doi.org/10.1029/2005GL024987

Eggleston, S., & Galbraith, E. D. (2018). The devil's in the disequilibrium: Multi-component analysis of dissolved carbon and oxygen changes under a broad range of forcings in a general circulation model. *Biogeosciences*, *15*(12), 3761–3777. https://doi.org/10.5194/bg-15-3761-2018

Friedlingstein, P., O'Sullivan, M., Jones, M., Andrew, R., Bakker, D., Hauck, J., et al. (2023). Global carbon budget 2023. *Earth System Science Data*, *15*(12), 5301–5369. https://doi.org/10.5194/essd-15-5301-2023

Galbraith, E. D., & Martiny, A. C. (2015). A simple nutrient-dependence mechanism for predicting the stoichiometry of marine ecosystems. *Proceedings of the National Academy of Sciences*, *112*(27), 8199–8204. https://doi.org/10.1073/pnas.1423917112

Garcia, H. E., Weathers, K., Paver, C. R., Smolyar, I., Boyer, T. P., Locarnini, R. A., et al. (2018). World Ocean Atlas 2018, Volume 4: Dissolved Inorganic Nutrients (phosphate, nitrate and nitrate+nitrite, silicate) [DataSet]. *National Oceanic and Atmospheric Administration*, 35. https://www.ncei.noaa.gov/access/world-ocean-atlas-2018/.NOAAAtlasNESDIS84

Gattuso, J. P., Williamson, P., Duarte, C. M., & Magnan, A. K. (2021). The potential for ocean-based climate action: Negative emissions technologies and beyond. *Frontiers in Climate*, *2*, 37. https://doi.org/10.3389/fclim.2020.575716

Hauck, J., Köhler, P., Wolf-Gladrow, D., & Völker, C. (2016). Iron fertilisation and century-scale effects of open ocean dissolution of olivine in a simulated CO_2 removal experiment. *Environmental Research Letters*, *11*(2), 024007. https://doi.org/10.1088/1748-9326/11/2/024007

Henson, S. A., Laufkötter, C., Leung, S., Giering, S. L. C., Palevsky, H. I., & Cavan, E. L. (2022). Uncertain response of ocean biological carbon export in a changing world. *Nature Geoscience*, *15*(4), 248–254. https://doi.org/10.1038/s41561-022-00927-0

Holzer, M. (2022). The fate of oxygen in the ocean and its sensitivity to local changes in biological production. *Journal of Geophysical Research: Oceans*, *127*(8), e2022JC018802. https://doi.org/10.1029/2022JC018802

Holzer, M., & DeVries, T. (2022). Source-labeled anthropogenic carbon reveals a large shift of preindustrial carbon from the ocean to the atmosphere. *Global Biogeochemical Cycles*, *36*(10), e2022GB007405. https://doi.org/10.1029/2022GB007405

Holzer, M., Kwon, E. Y., & Pasquier, B. (2021). A new metric of the biological carbon pump: Number of pump passages and its control on atmospheric pCO_2. *Global Biogeochemical Cycles*, *35*(6), e2020GB006863. https://doi.org/10.1029/2020GB006863

Irvine, P. J., Kravitz, B., Lawrence, M. G., & Muri, H. (2016). An overview of the Earth system science of solar geoengineering. *Wiley Interdisciplinary Reviews: Climate Change*, *7*(6), 815–833. https://doi.org/10.1002/wcc.423

Ito, T., & Follows, M. J. (2013). Air-sea disequilibrium of carbon dioxide enhances the biological carbon sequestration in the Southern Ocean. *Global Biogeochemical Cycles*, *27*(4), 1129–1138. https://doi.org/10.1002/2013GB004682

Ito, T., Nenes, A., Johnson, M. S., Meskhidze, N., & Deutsch, C. (2016). Acceleration of oxygen decline in the tropical Pacific over the past decades by aerosol pollutants. *Nature Geoscience*, *9*(6), 443–447. https://doi.org/10.1038/ngeo2717

Kalnay, E., Kanamitsu, M., Kistler, R., Collins, W., Deaven, D., Gandin, L., et al. (1996). The NMC/NCAR 40-year reanalysis project [Dataset]. *Bulletin of the American Meteorological Society*, *77*(3), 437–471. https://doi.org/10.1175/1520-0477(1996)077<0437:tnyrp>2.0.co;2

Kelley, C. T. (2003). *Solving nonlinear equations with Newton's method*. (pp. 1–25). SIAM. https://doi.org/10.1137/1.9780898718898.ch1

Kwon, E. Y., Primeau, F. W., & Sarmiento, J. L. (2009). The impact of remineralization depth on the air-sea carbon balance. *Nature Geoscience*, *2*(9), 630–635. https://doi.org/10.1038/ngeo612

Liu, Y., Moore, J. K., Primeau, F., & Wang, W. (2023). Reduced CO_2 uptake and growing nutrient sequestration from slowing overturning circulation. *Nature Climate Change*, *13*(1), 83–90. https://doi.org/10.1038/s41558-022-01555-7

Marinov, I., Gnanadesikan, A., Sarmiento, J. L., Toggweiler, J. R., Follows, M., & Mignone, B. K. (2008). Impact of oceanic circulation on biological carbon storage in the ocean and atmospheric pCO_2. *Global Biogeochemical Cycles*, *22*(3), GB3007. https://doi.org/10.1029/2007GB002958

Marinov, I., Gnanadesikan, A., Toggweiler, J. R., & Sarmiento, J. L. (2006). The Southern Ocean biogeochemical divide. *Nature*, *441*(7096), 964–967. https://doi.org/10.1038/nature04883

Martin, J. W., Knauer, G. A., Karl, D. M., & Broenkow, W. W. (1987). VERTEX: Carbon cycling in the NE Pacific. *Deep Sea Research Part A. Oceanographic Research Papers*, *34*(2), 267–285. https://doi.org/10.1016/0198-0149(87)90086-0

Moore, C. M., Mills, M. M., Arrigo, K. R., Berman-Frank, I., Bopp, L., Boyd, P. W., et al. (2013). Processes and patterns of oceanic nutrient limitation. *Nature Geoscience*, *6*(9), 701–710. https://doi.org/10.1038/NGEO1765

Moore, J. K., Fu, W., Primeau, F., Britten, G. L., Lindsay, K., Long, M., et al. (2018). Sustained climate warming drives declining marine biological productivity. *Science*, *359*(6380), 1139–1143. https://doi.org/10.1126/science.aao6379

NASEM. (2019). *Negative emissions technologies and reliable sequestration: A research agenda*. National Academies of Sciences, Engineering, and Medicine; The National Academies Press. https://doi.org/10.17226/25259

NCI-ESGF. (2013). NCI Earth System Grid Federation node CMIP5 archive [Dataset]. *NCI*. Retrieved from https://esgf.nci.org.au/projects/esgf-nci/

Nowicki, M., DeVries, T., & Siegel, D. A. (2022). Quantifying the carbon export and sequestration pathways of the ocean's biological carbon pump. *Global Biogeochemical Cycles*, *36*(3), e2021GB007083. https://doi.org/10.1029/2021GB007083

Nowicki, M., DeVries, T., & Siegel, D. A. (2024). The influence of air-sea CO_2 disequilibrium on carbon sequestration by the ocean's biological pump. *Global Biogeochemical Cycles*, *38*(2), e2023GB007880. https://doi.org/10.1029/2023GB007880

Pasquier, B. (2023). Code and data for: Optimal parameters for the ocean's nutrient, carbon, and oxygen cycles compensate for circulation biases but replumb the biological pump (v1.0.0) [Software]. *Zenodo*. https://doi.org/10.5281/zenodo.8067684

Pasquier, B., & Holzer, M. (2017). Inverse-model estimates of the ocean's coupled phosphorus, silicon, and iron cycles. *Biogeosciences*, *14*(18), 4125–4159. https://doi.org/10.5194/bg-14-4125-2017

Pasquier, B., Holzer, M., Chamberlain, M., Matear, R., Bindoff, N., & Primeau, F. (2023). Optimal parameters for the ocean's nutrient, carbon, and oxygen cycles compensate for circulation biases but replumb the biological pump. *Biogeosciences*, *20*(14), 2985–3009. https://doi.org/10.5194/bg-20-2985-2023

Pasquier, B., Holzer, M., & Chamberlain, M. A. (2023). The ocean's biological and preformed carbon pumps in future steady-state climate scenarios. *EGUsphere*, *2023*, 1–41. https://doi.org/10.5194/egusphere-2023-2525

Primeau, F. W., Holzer, M., & DeVries, T. (2013). Southern Ocean nutrient trapping and the efficiency of the biological pump. *Journal of Geophysical Research*, *118*(5), 2547–2564. https://doi.org/10.1002/jgrc.20181

Revelle, R., & Suess, H. E. (1957). Carbon dioxide exchange between atmosphere and ocean and the question of an increase of atmospheric CO_2 during the past decades. *Tellus*, *9*(1), 18–27. https://doi.org/10.3402/tellusa.v9i1.9075

Sabine, C. L., Feely, R. A., Gruber, N., Key, R. M., Lee, K., Bullister, J. L., et al. (2004). The ocean sink for anthropogenic CO_2. *Science*, *305*(5682), 367–371. https://doi.org/10.1126/science.1097403

Siegel, D. A., Buesseler, K. O., Behrenfeld, M. J., Benitez-Nelson, C. R., Boss, E., Brzezinski, M. A., et al. (2016). Prediction of the export and fate of global ocean net primary production: The EXPORTS science plan. *Frontiers in Marine Science*, *3*, 22. https://doi.org/10.3389/fmars.2016.00022

Siegel, D. A., DeVries, T., Doney, S. C., & Bell, T. (2021). Assessing the sequestration time scales of some ocean-based carbon dioxide reduction strategies. *Environmental Research Letters*, *16*(10), 104003. https://doi.org/10.1088/1748-9326/ac0be0

Toggweiler, J. R., Murnane, R., Carson, S., Gnanadesikan, A., & Sarmiento, J. L. (2003). Representation of the carbon cycle in box models and GCMs 2. Organic pump. *Global Biogeochemical Cycles*, *17*(1), 1027. https://doi.org/10.1029/2001GB001841

Volk, T., & Hoffert, M. I. (1985). Ocean carbon pumps: Analysis of relative strengths and efficiencies in ocean-driven atmospheric CO_2 changes. In E. T. Sundquist & W. S. Broecker (Eds.), *The carbon cycle and atmospheric CO_2: Natural variations Archean to present*, *Geophysical Monograph Series* (Vol. 32, pp. 99–110). AGU. https://doi.org/10.1029/GM032p0099

Weijer, W., Cheng, W., Garuba, O. A., Hu, A., & Nadiga, B. T. (2020). CMIP6 models predict significant 21st century decline of the Atlantic meridional overturning circulation. *Geophysical Research Letters*, *47*(12), e2019GL086075. https://doi.org/10.1029/2019GL086075

Wolf-Gladrow, D. A., Zeebe, R. E., Klaas, C., Körtzinger, A., & Dickson, A. G. (2007). Total alkalinity: The explicit conservative expression and its application to biogeochemical processes. *Marine Chemistry*, *106*(1–2), 287–300. https://doi.org/10.1016/j.marchem.2007.01.006